Raman spectra of $(Rb_x(NH_4)_{1-x})_2SO_4$ crystals

1998 J. Phys.: Condens. Matter 10 1157

(http://iopscience.iop.org/0953-8984/10/5/023)

J. Phys.: Condens. Matter **10** (1998) 1157–1173. Printed in the UK PII: S0953-8984(98)85034-0

Raman spectra of $(Rb_x(NH_4)_{1-x})_2SO_4$ crystals

Yu I Yuzyuk†‡§, V I Torgashev†, R Farhi‡, I Gregora§, J Petzelt§, P Simon‖, D De Sousa Meneses‖ and L M Rabkin†

† Institute of Physics, Rostov State University, Stachki 194, 344090, Rostov-on-Don, Russia
‡ Laboratoire de Physique de la Matière Condensée, Université de Picardie Jules Verne, 33, rue Saint-Leu, 80039 Amiens Cédex, France
§ Institute of Physics, Academy of Sciences of the Czech Republic, Na Slovance 2, 180 40 Prague 8, Czech Republic
‖ Centre de Recherche sur la Physique des Hautes Temperatures, F-45071 Orléans Cédex, France

Received 9 June 1997, in final form 7 November 1997

Abstract. Polarized Raman spectra of $(Rb_x(NH_4)_{1-x})_2SO_4$ crystals ($x = 0.1$ and 0.7) were studied in the temperature range 10–300 K. Thorough site-symmetry analysis of internal SO_4^{2-} and NH_4^+ vibrations combined with factor-group analysis based on hexagonal pseudosymmetry allowed us to make an assignment of the observed modes. The spectra of the $x = 0.1$ sample are compatible with those of pure $(NH_4)_2SO_4$ including the features of the disorder in the paraelectric phase above 220 K (the broad central peak of the relaxator type and high mode damping) and ordering in the ferroelectric phase. The spectra of the $x = 0.7$ sample show a much smaller disorder at high temperatures (no broad central mode and lower mode damping) due to the lower ammonium content, but clearly confirm the onset of the dynamic dipolar glass transition (short-range correlations inducing the appearance of long-lived dipolar clusters) near 220 K.

1. Introduction

Ammonium sulphate ($(NH_4)_2SO_4$, hereafter denoted as AS) undergoes a first-order ferroelectric phase transition (PT) $Pnma$ (D_{2h}^{16}) $\rightarrow$ $Pn2_1a$ (C_{2v}^9) at $T_C = 223$ K. It represents a classical example of a weak ferroelectric with a very small Curie–Weiss constant and small spontaneous polarization with a peculiar temperature behaviour. The PT mechanism was determined recently and also the behaviour of the spontaneous polarization was explained (De Sousa Meneses *et al* 1995).

The mixed crystals $(Rb_x(NH_4)_{1-x})_2SO_4$ (denoted as RbAS-100x) were studied and discussed as much as 20 years ago, but there was no indication of any glassy behaviour. As was found by Ohi *et al* (1978), isomorphic substitution of ions with close values of ionic radii, NH_4^+ and Rb^+, leads to slight changes in the lattice constants of RbAS-100x crystals, while with increasing Rb^+ concentration the PT temperature rises by a few degrees until, at a certain concentration $x = 0.24$, it starts to drop down abruptly. The Curie–Weiss constant increases gradually and the PT changes its character from first order to second order at a certain concentration x. No PTs have been detected for mixed crystals with $x > 0.6$ upon cooling down to liquid helium temperature.

Recently, evidence for orientational glass behaviour has been found for RbAS mixed crystals for x-values close to that of rubidium sulphate ($x = 0.7$) by means of IR and dielectric measurements (De Sousa Meneses 1995, De Sousa Meneses *et al* 1995). From

0953-8984/98/051157+17$19.50

the analysis of the low-frequency dielectric data, the orientational glass state in RbAS-70 is characterized by a rather broad distribution of relaxations, and in IR spectra some internal modes of the sulphate group start to appear much better resolved below 200 K.

The present contribution reports on a comparative Raman study of two representatives of the family of mixed sulphates: RbAS-10 and RbAS-70.

2. Crystal structure and symmetry analysis

At room temperature, RbAS-100x mixed crystals as well as pure compounds possess the orthorhombic β-K_2SO_4-type structure $Pnma$ with four formula units in the primitive cell (Ohi *et al* 1978). Sulphur atoms occupy 4(c) Wyckoff positions (site symmetry C_s). Two oxygen atoms of each SO_4^{2-} ion, namely O(1) and O(2), are also at 4(c) positions, while the other two oxygen atoms (labelled as O(3)) of the SO_4^{2-} ion are crystallographically equivalent, occupying 8(d) positions. There are two non-equivalent cations, NH_4^+(I) and NH_4^+(II), which occupy 4(c) positions, too. Consequently, all of the ions occupy sites on the mirror plane of C_s symmetry in the paraelectric phase, while in the ferroelectric phase of pure AS both kinds of ammonium and sulphate ion occupy fourfold positions with C_1 site symmetry (Schlemper and Hamilton 1966, Hasebe 1981, Ahmed *et al* 1987).

The distribution of rubidium between the two non-equivalent ammonium sites in mixed crystals (nominally $x = 0.52$) has been determined by x-ray diffraction. At room temperature the ratio of the occupation numbers was Rb(I)/Rb(II) = 0.41/0.62. Therefore, the substitution is preferentially on one sublattice (Unruh *et al* 1978).

The factor-group analysis of normal vibrations for pure AS is well known for the $Pnam$ setting of the D_{2h}^{16} space group (Torrie *et al* 1972, Petzelt *et al* 1973, Venkateswarlu *et al* 1975, Carter 1976, De Sousa Meneses *et al* 1995). Hereafter we use *standard notation*—$Pnma$. This change necessitates using labels different from those used by the authors cited above, who have reported single-crystal Raman and IR data. The correspondence of the irreducible representation labels between these two settings is as follows:

$$(Pnam \rightarrow Pnma): \qquad B_{1g,u} \rightarrow B_{2g,u};\ B_{2g,u} \rightarrow B_{3g,u};\ B_{3g,u} \rightarrow B_{1g,u}.$$

Detailed investigations of polarized Raman and IR spectra of AS (see the papers cited above) showed a discrepancy between the number of modes predicted by the factor-group analysis and that actually observed. In the paraelectric phase some internal modes of SO_4^{2-} and NH_4^+ ions, symmetry allowed only in the ferroelectric phase, are nevertheless present because of a dynamical breaking of the local symmetry of the SO_4^{2-} and NH_4^+ tetrahedra. As demonstrated by Kozlov *et al* (1988), the presence of a strong disorder in AS is obvious. In fact, the local and instantaneous site symmetry of SO_4^{2-} and NH_4^+ tetrahedral ions above T_C is C_1, which is the same symmetry as that below T_C, whereas the C_s sites correspond to average positions in the paraelectric phase.

The isomorphic substitution $Rb^+ \rightarrow NH_4^+$ does not change the factor-group symmetry, but leads to pronounced perturbations in the local symmetry of both SO_4^{2-} and NH_4^+ tetrahedra in mixed crystals, since each NH_4^+ ion is bound via asymmetric N–H...O bonds with the O atoms of SO_4^{2-} groups. These induced distortions of the tetrahedra in the unit cell and their shift away from the C_s sites should manifest themselves in the vibration spectra of mixed crystals. Furthermore, as shown in the Raman (Yuzyuk *et al* 1995, 1996) and IR (Simon 1992) studies of KDP-type glasses, the distortions in the glass state are more pronounced and lead to splitting of some lines and stronger relaxation of the selection rules in the Raman and IR spectra.

It is known (Torgashev *et al* 1988, 1991, 1992, 1993) that some peculiarities of the room temperature Raman spectra of β-K_2SO_4-type crystals follow from the pseudo-hexagonal character of the crystal structure. In 1976, Sawada *et al* introduced a hypothetical prototypic (latent) phase of $P6_3/mmc$ symmetry (α-K_2SO_4-type structure) for AS. Later, a method of assignment of the vibration spectra for β-K_2SO_4-type crystals was developed by Torgashev *et al* (1992) considering the genesis of real spectra from the spectra of the prototypic phase at the hypothetical antiferrodistortive transition $P6_3/mmc \rightarrow Pnma$.

The prototypic α-K_2SO_4-type structure has a hexagonal lattice of $P6_3/mmc$ symmetry with two formula units in the unit cell. As assumed for AS (Torgashev *et al* 1988), the ions occupy the following sites:

NH_4^+ (I)	2(d); D_{3h}
NH_4^+ (II)	2(a); D_{3d}
SO_4^{2-}	2(c); D_{3h}.

The necessary condition for the existence of this structure is the orientational mobility of the anion sublattice (at any given moment, the SO_4^{2-} ions occupy the f position of C_{3v} symmetry). The formation of the real phase of $Pnma$ symmetry from the latent phase of $P6_3/mmc$ symmetry takes place at the PT together with the doubling of the unit-cell volume. This PT is induced by an order parameter transforming according to the M_4 representation from the M point of the hexagonal Brillouin zone. Thus the spectra of the $Pnma$ phase will be formed from the modes of the Γ and M points of the $P6_3/mmc$ phase.

On the basis of analogous considerations, the genesis of the IR and Raman spectra of external modes and detailed assignments were given for several crystals with β-K_2SO_4-type structure (Torgashev *et al* 1992, 1993). This approach will be used below to describe the observed room temperature Raman spectra of RbAS-10 and RbAS-70 in the region of internal vibrations.

3. Experimental details

The crystals were grown by slow cooling from aqueous solution. Polarized Raman spectra have been measured for samples in the form of carefully oriented and optically polished rectangular parallelepipeds, $4 \times 3 \times 2$ mm^3. The sample was placed in a continuous-flow cryostat (LEYBOLD VSK 4-300) where it was convection cooled in He exchange gas. Special care was taken to ensure identical experimental conditions for the two samples. The 514.5 nm Ar^+ laser line at 200 mW was used for excitation in the right-angle scattering geometry. The scattered light was analysed using a PC-controlled double-grating spectrometer (SPEX-14018) equipped with a standard single-channel photon-counting detection system. The spectral slit width was set to 1 cm^{-1} or 2 cm^{-1} (below and above 1200 cm^{-1}, respectively).

4. Results and discussion

4.1. Raman spectra at room temperature

The overall Raman spectra of RbAS-10 and RbAS-70 at 290 K for six different scattering geometries are shown in figures 1 and 2, respectively, and the corresponding frequencies and assignment are summarized in tables 1 and 2. The fundamental internal vibrations of NH_4^+ and SO_4^{2-} ions allowed under the T_d point group consist of one non-degenerate

Table 1. Frequencies (in cm^{-1}) of the observed Raman lines for RbAS-70 (vs: very strong; s: strong; w: weak; vw: very weak).

$Z(XX)Y$ A_g	$Z(YY)X$ A_g	$Y(ZZ)X$ A_g	$Y(XY)X$ B_{1g}	$Y(XZ)X$ B_{2g}	$Y(ZY)X$ B_{3g}	Assignment
44		**45***		45 vw		
66	**67***	**69***	**63***		**61***	t^S
			73	**71***		
	78*	**79***			**78***	
120 vw	**119* vw**	113	120	**120* vw**	**115***	l^S
		130*				
183 vw	170 vw	181				t^N
					196	
444	**445***	**446***		**450* s**		ν_2^S (451)
		452	**453***		**453***	
	615* s	**615* s**				
			618*	**617***	**617***	ν_4^S (615)
622 s	**623***	**623***		**630***		
961* vw	**961* vw**	**961* vw**				
976* vs	**976* vs**	**976* vs**	**976* vw**	**976* w**	**976* vw**	ν_1^S (981)
	1081*	**1082***				
	1090*	**1091***			1090	ν_3^S (1105)
			1100*	**1101***	**1100***	
1130	**1130***	**1131***		1132		
1230	1230	1230				$2\nu_4^S$
1422	1420	1425	1425	1422	1425	
1449	1455					ν_4^N (1400)
		1473		1473 vw		
1665		1668				ν_2^N (1680)
	1686		1686	1680	1692	
2870	2880	2870		2840	2850	$2\nu_4^N$
	3045	3021		3027		ν_1^N (3040)
			3050		3042	
3135	3114	3118				$\nu_2^N + \nu_4^N$
		3193	3190		3186	ν_3^N (3145)
3210	3204			3225		
		3318				
3350 w	3350 w					$2\nu_2^N$

* The peak positions (bold typeface) coincide with those observed for pure Rb_2SO_4.

fully symmetric stretching mode $\nu_1(A_1)$, one doubly degenerate bending mode $\nu_2(E)$, one triply degenerate asymmetric stretching mode $\nu_3(F_2)$ and one triply degenerate bending mode $\nu_4(F_2)$. The frequencies of these modes in free ions (Nakamoto 1986) are given in the right-hand columns of tables 1 and 2 (values in brackets). Following the notation used by Venkateswarlu *et al* (1975), the modes of the NH_4^+ and SO_4^{2-} ions have been labelled with the superscripts N and S respectively. The Herzberg notation ν_i has been used for internal modes of these ions and the symbols t and l for their translations and

Table 2. Frequencies (in cm^{-1}) of the observed Raman lines for RbAS-10 (vs: very strong; s: strong; w: weak; vw: very weak).

$Z(XX)Y$ A_g	$Z(YY)X$ A_g	$Y(ZZ)X$ A_g	$Y(XY)X$ B_{1g}	$Y(XZ)X$ B_{2g}	$Y(ZY)X$ B_{3g}	Assignment
43		44				
				65	66	t^S
	75	77	75			
79 vw				83	83	
119	114	112				l^S
	174		162		176	t^N
185		181		187		
		203			197	
448	447	448		450 s		ν_2^S (451)
		453	453		453	
	613 s	613 s				
			618	617	615	ν_4^S (615)
625 s	625	625		631		
961 vw	961 vw	961 vw				
976 vs	976 vs	976 vs	976 vw	976 w	976 vw	ν_1^S (981)
	1067	1067				
1074						
			1094	1088	1087	ν_3^S (1105)
1118	1116	1116				
1230	1230	1230				$2\nu_4^S$
	1404					
1416		1416	1413	1419	1425	ν_4^N (1400)
1449	1455					
		1473		1480 vw		
1665		1662	1674	1674		ν_2^N (1680)
	1686				1692	
2870	2880	2870		2840	2850	$2\nu_4^N$
	3042	3021		3018		ν_1^N (3040)
			3050		3042	
3135	3114	3118				$\nu_2^N + \nu_4^N$
3186		3193	3190		3186	ν_3^N (3145)
	3204			3200		
		3307				
3350 w	3350 w					$2\nu_2^N$

librations, respectively.

A quick glance at the Raman spectra of RbAS-10 and RbAS-70 shows that the room temperature spectra of RbAS-70 (below 1200 cm^{-1}) are close to those of pure Rb_2SO_4 (Montero *et al* 1973) whereas the spectra of RbAS-10 are close to those of pure AS (Venkateswarlu *et al* 1975) within the experimental error of ± 2 cm^{-1}. The frequencies of the lines in the spectra of RbAS-70 coinciding with the corresponding lines of pure Rb_2SO_4 crystals are marked with asterisks in table 1.

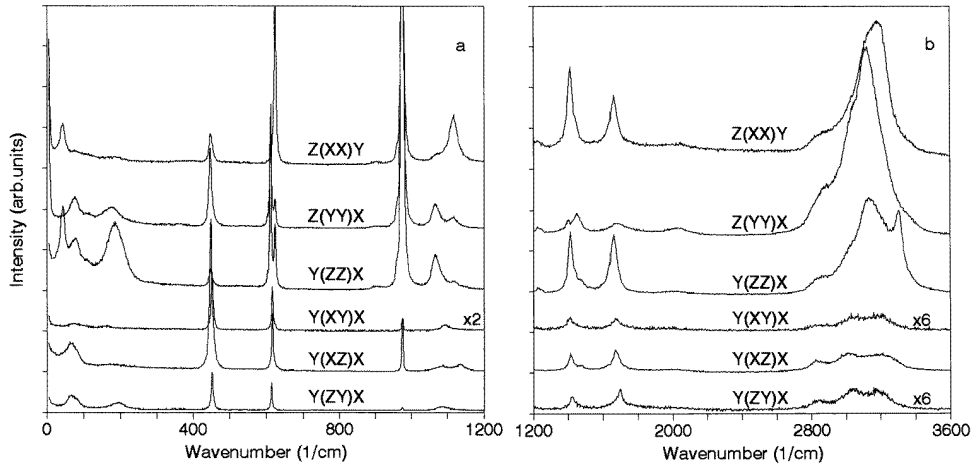

Figure 1. Overall Raman spectra of RbAS-10 at room temperature for six polarization geometries.

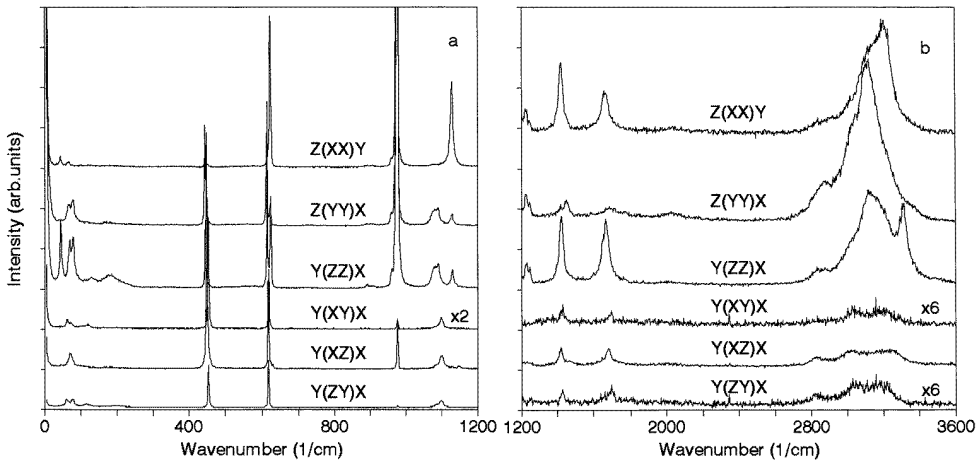

Figure 2. Overall Raman spectra of RbAS-70 at room temperature for six polarization geometries. The intensities of the spectra above 1200 cm^{-1} in (b) were multiplied by a factor of 3 in comparison with those of figure 1(b).

4.1.1. Internal modes of SO_4^{2-}. As predicted by the factor-group analysis of the ideal β-K_2SO_4 structure (D_{2h}^{16} space group), the fully symmetric stretching vibration ν_1^S of the SO_4^{2-} ion should be observable only in the A_g and B_{2g} spectra. In pure Rb_2SO_4 this mode was observed at 976 cm^{-1} (Montero *et al* 1973) in A_g spectra only, whereas in pure AS, RbAS-10 and RbAS-70, a leakage of the ν_1^S mode (at the same frequency, 976 cm^{-1}) into geometries corresponding to B_{1g} and B_{3g} is detected. A forbidden internal mode, ν_1^S, was also observed in the IR reflectivity spectra of the paraelectric phase of pure AS (De Sousa Meneses *et al* 1995). The leakage of the ν_1^S mode into B_{1g} and B_{3g} geometries is possible only if the SO_4^{2-} ions exhibit C_1 local symmetry (obviously of dynamic origin) even at room temperature. The ν_1^S mode is allowed for all Raman scattering geometries and for

all IR polarizations in the ferroelectric phase of pure AS. However, its intensity does not change very much at the phase transition from a paraelectric to a ferroelectric phase (De Sousa Meneses *et al* 1995), in which the SO_4^{2-} ions have C_1 local symmetry. Hence, the leakage of the ν_1^S mode observed by us cannot be due to errors in the scattering geometries or spillover of the polarizer.

A very weak band at 961 cm^{-1} (15 cm^{-1} lower than the very intense line corresponding to the ν_1^S mode) was also observed by Montero *et al* (1973) in the Raman spectra of orthorhombic sulphates, and can be assigned to the ν_1 mode of the isotopic ions $(S^{16}O_3^{18}O)^{2-}$. The intensity of the ^{18}O ν_1 band relative to that of the ^{16}O one gives the result 0.25×10^{-2}, which is quite close to the natural ^{18}O:^{16}O abundance ratio: 0.203×10^{-2}.

The doubly degenerate ν_2^S bending mode should be present as a single line in all of the scattering geometries. The Raman spectra of RbAS-70 follow the factor-group predictions, and the frequencies of the corresponding lines have values very close to those of pure Rb_2SO_4 crystal (see table 1). On the other hand, the room temperature Raman spectra of RbAS-10 in the ν_2^S region closely resemble those of pure AS studied by Venkateswarlu *et al* (1975) and Carter (1976), except for an additional forbidden peak near 453 cm^{-1}. This peak could originate from the B_{1g} and/or B_{3g} strong component of the ν_2^S mode leaking into A_g spectra as a result of disorder of SO_4^{2-} tetrahedra.

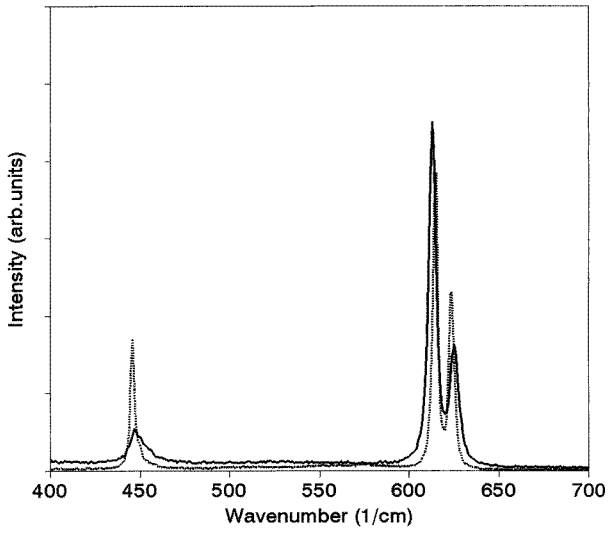

Figure 3. Raman spectra in the $Y(ZZ)X$ scattering geometry of RbAS-10 (solid line) and RbAS-70 (dotted line) in the region of the ν_2^S and ν_4^S internal modes.

The triply degenerate bending vibration ν_4^S should show two components in both A_g and B_{2g} spectra and single lines in B_{1g} and B_{3g} spectra. The Raman spectra of RbAS-10 and RbAS-70 at 290 K for $Y(ZZ)X$ scattering geometry (A_g modes) in the ν_2^S–ν_4^S region are displayed in the figure 3. The number of lines observed for both crystals in the region of ν_4^S is in agreement with the factor-group analysis, but important differences between the spectra of these crystals should be pointed out.

(i) The doublet corresponding to ν_4^S in RbAS-70 has two components at 615 and 623 cm^{-1} in the $Y(ZZ)X$ orientation, while in RbAS-10 the splitting is much more pronounced: the two components are at 613 and 625 cm^{-1}. Such an increase of the mode

splitting is direct evidence of the fact that the magnitude of the distortion of the sulphate tetrahedra is considerably larger in RbAS-10.

(ii) Significant broadening of all internal vibrations of SO_4^{2-} ions with increasing ammonium concentration implies that *ammonium disorder increases the anharmonicity of the sulphate sublattice in the paraelectric phase*.

The asymmetric stretching mode ν_3^S is strongly dipole active, and strong intermolecular coupling of ν_3^S might be expected. Torrie *et al* (1972) have reported that the Raman peak centred at 1106 cm^{-1} in AS shifts down to 1056 cm^{-1} in deuterated crystal because of hetero-ionic vibrational coupling between deuteroammonium and sulphate modes. Raman spectra of RbAS-10 and RbAS-70 in the region of the ν_1^S and ν_3^S modes for the $Y(ZZ)X$ orientation are presented in figure 4. Besides the broadening mentioned above, a considerable shift is observed, due to the strong sensitivity of ν_3^S to the distortions induced by ammonium. A discrepancy between factor-group predictions and the observed Raman spectra in the ν_3^S region is obvious: instead of the two A_g lines predicted, three well-defined peaks at 1081, 1090 and 1130 cm^{-1} were observed in RbAS-70 ($Z(YY)X$ and $Y(ZZ)X$ geometries). All three components of the triply degenerate ν_3^S mode appear because of the disorder of sulphate ions, as mentioned above.

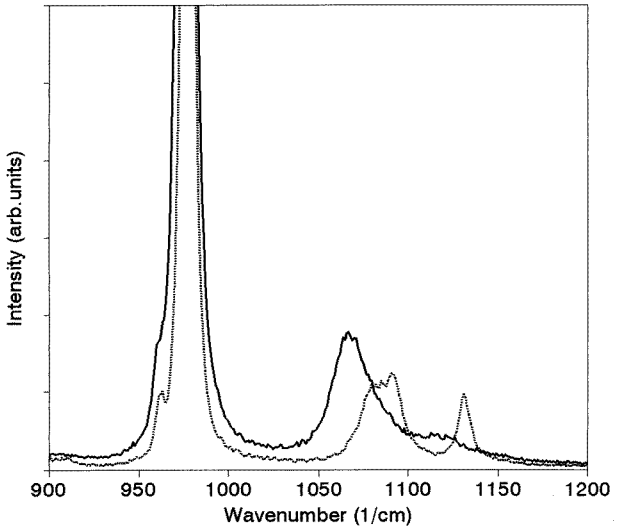

Figure 4. Raman spectra in the $Y(ZZ)X$ scattering geometry of RbAS-10 (solid line) and RbAS-70 (dotted line) in the region of the ν_1^S and ν_3^S internal modes.

The overall Raman spectra of internal vibrations of the sulphate ions in RbAS-70 as well as in RbAS-10 have a common specific feature: *the polarization character corresponds to the hexagonal class*. As is known, the x-axis is pseudo-hexagonal in the room temperature phase of $Pnma$ symmetry. The Raman tensor component α_{XX} for the D_{6h} class corresponds to A_g^h modes (the superscript h is used to mark hexagonal symmetry species), while α_{YY} and α_{ZZ} correspond to $A_g^h + E_{2g}^h$ modes. So, the Raman spectra for the two crystals are quite close for $Y(ZZ)X$ and $Z(YY)X$ geometries, while the $Z(XX)Y$ spectra differ appreciably. Since tetrahedral SO_4^{2-} ions occupy sites of C_{3v} symmetry in the latent hexagonal phase, the site-symmetry splitting of the triply degenerate modes $F_2 \rightarrow A_g^h + E_{2g}^h$ mode is approximately obeyed in the room temperature phase, too. For RbAS-70, the single peak at 1130 cm^{-1} for

the $Y(XX)Z$ orientation arises from the A_g^h component of the ν_3^S mode, while the doublet at 1081–1090 cm^{-1} obviously originates from the E_{2g}^h component. The site-symmetry splitting of the E_{2g} pair is about 9 cm^{-1} and the A_g–E_{2g} site-symmetry splitting is larger, i.e. 45 cm^{-1}. The A_g component is observed at the highest frequency (1130 cm^{-1}), and the intensity of this peak follows the rule $I(xx) > I(yy) \simeq I(zz)$. For the E_{2g} doublet (1081 and 1090 cm^{-1}) the intensity is also in accordance with the hexagonal class: $I(yy) \simeq I(zz)$ and $I(xx) = 0$. For RbAS-10 the same feature was observed for the ν_3^S mode, where no splitting of the E_{2g}^h doublet was detected, probably because of the broadening discussed above. Its asymmetrical lineshape, however, suggests the presence of an unresolved doublet.

The triply degenerate ν_4^S mode also exhibits pseudo-hexagonal features but with a weak A–E splitting (less than 1 cm^{-1}), while the E_{2g}^h doublet appears at 613 and 625 cm^{-1} for RbAS-10 and at 615–623 cm^{-1} for RbAS-70. The intensities of the singlets corresponding to ν_2^S in RbAS-70 also attest to a hexagonal origin, i.e. $I(zz) \simeq I(yy)$, $I(xx) \simeq 0$. For RbAS-10, $I(xx)$ for the ν_2^S mode at 448 cm^{-1} is considerably larger, while $I(zz)$ is less than $I(yy)$, probably because of a more pronounced disorder in this crystal.

4.1.2. Internal modes of NH_4^+. The Raman spectra of RbAS-10 and RbAS-70 in the region of internal vibrations of NH_4^+ ions (1400–3500 cm^{-1}) closely resemble those of pure AS for all scattering geometries. The absolute values of the peak frequencies, given in tables 1 and 2, do not differ by more than 1%. In accordance with the ammonium content in the samples, the intensity of these bands in RbAS-10 is three times as high as that for RbAS-70. The region of ν_1^N–ν_3^N is the most difficult to interpret because of the Fermi resonance with overtones $2\nu_2^N$, $\nu_2^N + \nu_4^N$ and $2\nu_2^N$. The assignment given in tables 1 and 2 is based on the analysis of the spectra of pure AS carried out by Venkateswarlu *et al* (1975).

Like the SO_4^{2-} modes, the NH_4^+ modes exhibit a leakage into other geometries because of a lower local symmetry. The leakage looks more progressive than that of the SO_4^{2-} ions, evidently due to the considerable departure of NH_4^+ ions from the mirror plane in those vibrations which exhibit strong anharmonicity. The observations mentioned above lead to the following conclusion: in the mixed crystals RbAS-10 (with high NH_4^+ content) and RbAS-70 (with low NH_4^+ content), ammonium ions exhibit the same behaviour as in pure AS, and local ferroelectric correlations might be expected to appear in RbAS-70 on cooling.

4.1.3. External vibrations. The low-frequency Raman spectra of the external vibrations of RbAS-10 were studied by Torgashev *et al* (1988) in connection with the ferroelectric PT, and an assignment of all of the external modes was given. The Raman spectra of RbAS-70 below 130 cm^{-1} are close to those of pure Rb_2SO_4. Also, the additional weak bands present at 170–200 cm^{-1} relate to the translations of the ammonium ions. It is known that the librations of ammonium exhibit very strong damping due to strong disorder at room temperature, and were observed only in the ferroelectric phase of AS (Iqbal and Christoe 1976).

Like for the internal vibrations of SO_4^{2-} ions, direct evidence of the fact that ammonium disorder induces a disorder of the sulphate anions is presented in figure 5. Besides a strong broadening of all of the external modes of SO_4^{2-} ions, an appreciable central component appears in the Raman spectra of RbAS-10. The low-frequency Raman response of RbAS-10 in the $Y(ZZ)X$ orientation (A_g species) at 290 K was well fitted by a sum of six damped harmonic oscillators together with a Debye relaxator (accounting for the broad

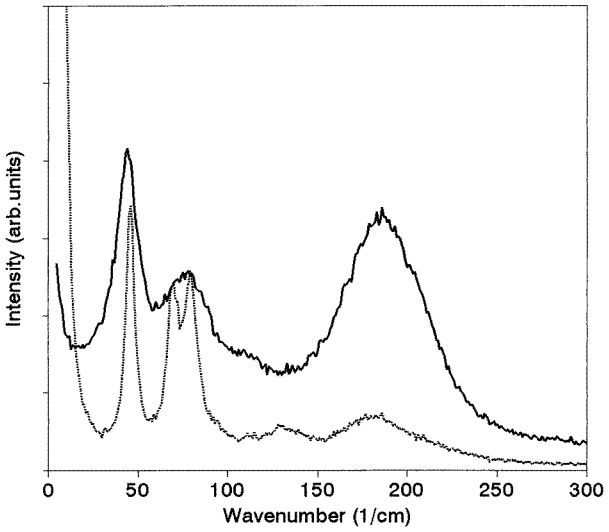

Figure 5. Raman spectra for the $Y(ZZ)X$ scattering geometry of RbAS-10 (solid line) and RbAS-70 (dotted line) in the region of external vibrations.

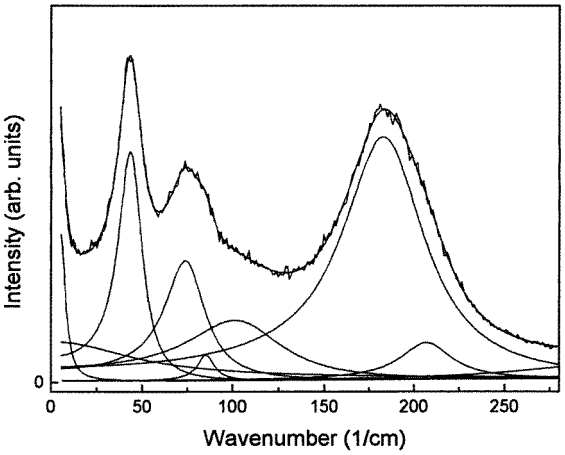

Figure 6. The decomposition of the room temperature $Y(ZZ)X$ Raman spectra of RbAS-10 (damped classical oscillators + Debye relaxator) as obtained by fitting.

central component) according to the formula

$$I(\omega, T) \approx (1 + n(\omega, T)) \left[A_R \frac{\omega\tau_R}{1 + (\omega\tau_R)^2} + \sum_j A_{Oj} \frac{\omega\Omega_{Oj}^2 \Gamma_{Oj}}{(\Omega_{Oj}^2 - \omega^2)^2 + (\omega\Gamma_{Oj})^2} \right]. \tag{1}$$

Here $n(\omega, T)$ is the Bose–Einstein factor; A_{Oj}, Ω_{Oj} and Γ_{Oj} are the strength, frequency and damping of the jth oscillator; A_R and Γ_R are the strength and relaxation time of the Debye relaxator. For the purpose of the fit, the Rayleigh scattering wing (the apparatus function) at the lowest frequencies as well as the wing due to the integral contribution of the peaks at frequencies higher than 300 cm^{-1} were conveniently modelled by fixed

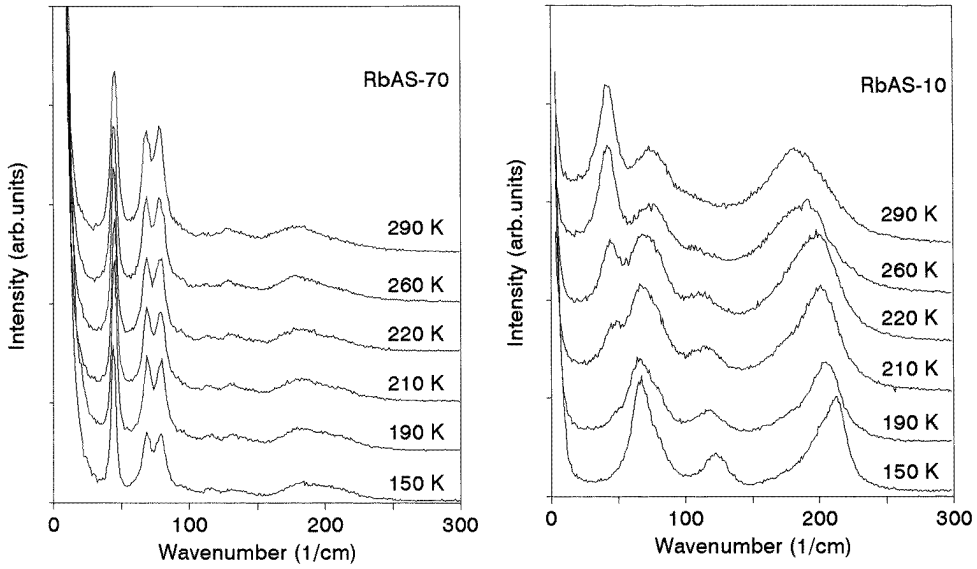

Figure 7. The temperature evolution of the low-frequency Raman spectra for the $Y(ZZ)X$ scattering geometry of RbAS-70 and RbAS-10 crystals.

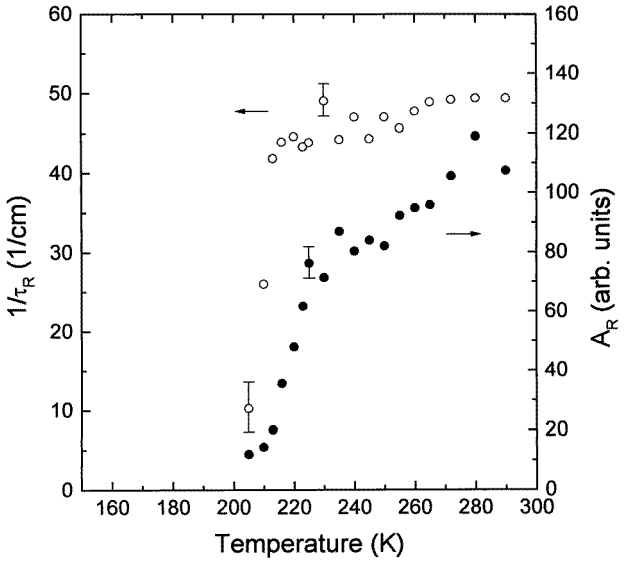

Figure 8. The temperature dependence of the relaxator parameters (strength A_R and reciprocal relaxation time $1/\tau_R$) for RbAS-10, as obtained by fitting.

Lorentzian components. The results are shown in figure 6. In contrast to those for RbAS-10, the spectra for RbAS-70 do not show any relaxator component, whereas the Rayleigh component, which corresponds to the elastic scattering, was found to have an approximately three-times-larger half-width.

4.2. Temperature evolution

4.2.1. External vibrations. The temperature evolution of the low-frequency Raman spectra of RbAS-10 and RbAS-70 ($Y(ZZ)X$ scattering geometry) is shown figure 7. On lowering the temperature, external vibrations (below 150 cm^{-1}) in RbAS-70 do not reveal any signature of a structural transformation. Some lines become much better resolved as a result of a natural decrease of their widths, which indicates a lowering of the anharmonicity of the thermal vibrations.

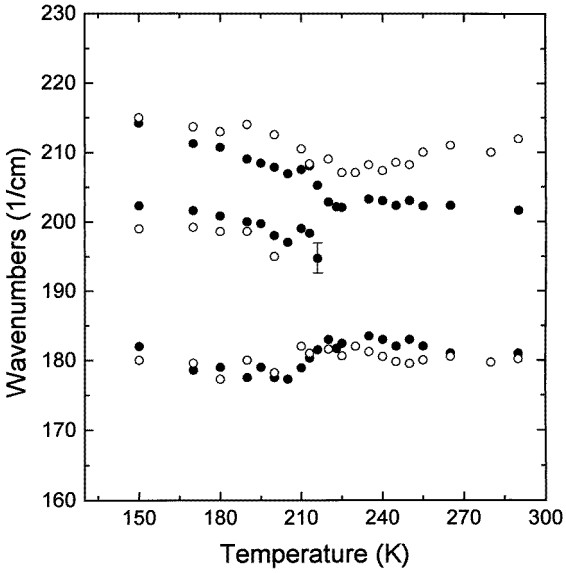

Figure 9. The temperature dependence of the frequencies of the ammonium translation modes in RbAS-10 (full symbols) and RbAS-70 (open symbols) obtained from the fit. A typical error bar is indicated.

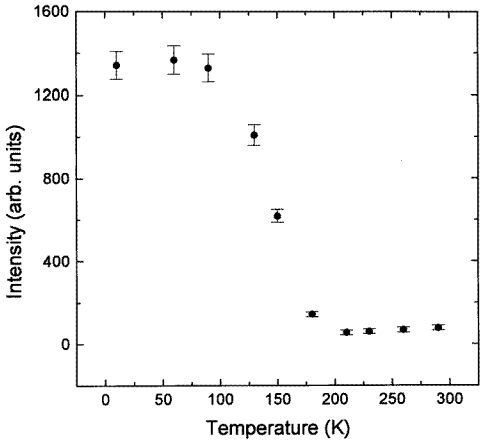

Figure 10. The temperature dependence of the integral intensity of the ν_1^S mode.

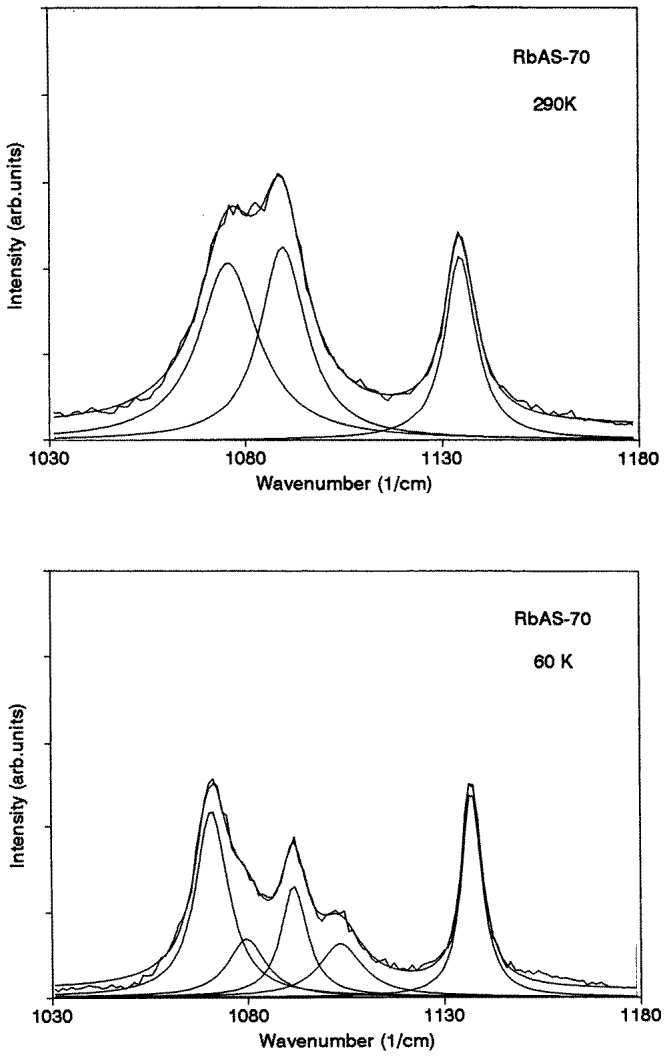

Figure 11. The decomposition into individual Lorentzian components of the Raman spectra of RbAS-70 at 290 and 60 K.

In contrast, the occurrence of the ferroelectric PT is obvious from the temperature behaviour of the external modes in RbAS-10: the temperature evolution observed in RbAS-10 is similar to that of pure AS. In particular, an abrupt reduction of the relaxator contribution and disappearance of the intense 44 cm^{-1} Ag line below $T_C = 226$ K was observed. The drastic decrease of the relaxator strength A_R and reciprocal relaxation time $1/\tau_R$, as found from the fits of the spectra in the frequency region 5–300 cm^{-1} using equation (1), is shown in figure 8. With temperature decreasing from 205 K, the relaxator component becomes too small to be reliably determined by the fitting procedure; its removal does not impair the quality of the overall fit. We note that the half-width and position of the central narrow Rayleigh line were fixed over the whole temperature interval. The disappearance of the broad central Raman component observed only for RbAS-10 is due to slowing

down (i.e. freezing) of the relaxation at the ferroelectric PT. Our results corroborate the microscopic origin of this relaxation assumed by Iqbal and Christoe (1976) and developed recently by De Sousa Meneses *et al* (1995)—namely that the central component arises as a result of anharmonic reorientations of the sulphate and ammonium ions. Similar effects were observed also in pure AS in the Raman (Unruh *et al* 1978) as well as in the submillimetre spectra (Kozlov *et al* 1988).

The translational modes of ammonium ions, located in the region 150–220 cm^{-1}, exhibit similar temperature dependences in the two crystals with nearly identical values of the peak positions. Above T_C the experimental spectra were fitted using two peaks, while at the lowest temperature (150 K) an additional peak at 200 cm^{-1} was included in the fitting procedure. Applying the fitting procedure over the entire temperature interval (150–290 K) we arrived at the following conclusion (see figure 9): the emergence of the third peak, which is a pronounced feature of the IR spectra for all three polarizations (Petzelt *et al* 1973), is located at 220 K for RbAS-10 and at a somewhat lower temperature (about 215 K) for RbAS-70. Thus, the onset of the formation of dipolar clusters in the ammonium-rich regions of RbAS-70 can be suggested to take place below 220 K.

4.2.2. Internal modes of SO_4^{2-}. On lowering the temperature, we observe further increase in the leakage of the modes in RbAS-70 due to freezing-in of SO_4^{2-} ions in general non-symmetric positions allowed for the ferroelectric phase. The observed changes in the Raman spectra of SO_4^{2-} ions are associated with a reduction of the local symmetry due to a gradual freezing-in of their orientational motions, with lifetimes longer than the characteristic time of a Raman scattering event. This gradual process is manifested as a gradual splitting of the spectral lines, while ν_1^S shows an intensity increase in the non-diagonal orientations on cooling. The intensity of the ν_1^S line for the $Y(ZY)X$ orientation, as shown in figure 10, markedly increases below 150 K, where high-frequency dielectric dispersion starts to set in.

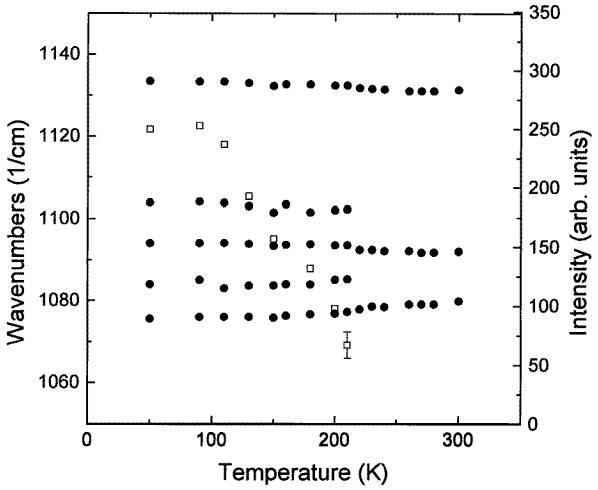

Figure 12. The temperature dependence of the frequencies (full symbols; the error bar is the same size as the symbols) of the decomposed Raman peaks shown in figure 11, and the integral intensity (open symbols; a typical error bar is indicated) of a line emerging at 1104 cm^{-1}.

Furthermore, we would like to point out a very important experimental fact established for RbAS-70. As shown recently by De Sousa Meneses *et al* (1996) for RbAS-70, the ν_3^S

doublet appears much better resolved below 200 K in the IR spectra of B_{2u} symmetry. We have carried out a detailed Raman study of a RbAS-70 sample in this spectral range with the following result. For the $Y(ZZ)X$ orientation (A_g modes), three lines were detected at 1082, 1091 and 1131 cm^{-1} in the room temperature spectrum. Two additional lines at 1084 and 1104 cm^{-1} appear on cooling below 220 K (see figure 11). The temperature dependences of their frequencies and of the integral intensity of the new 1104 cm^{-1} line are shown in figure 12. The parameters in this case were obtained using a simple multi-Lorentzian fit (which, in this spectral range, gives equivalent results to the harmonic oscillator model). The origin of these two additional lines is obvious: their frequencies coincide with the frequencies of two TO modes observed in the IR spectra of B_{2u} symmetry. Such an appearance of the IR-active modes in the Raman spectra is allowed by the selection rules for non-centrosymmetric ferroelectric phases owing to the following correlation between irreducible representations of $Pnma$ and $Pn2_1a$ groups:

$$\begin{array}{ccccc} & & A_g & & \\ & \searrow & & & \\ Pnma & & A_1(LO+TO) & & Pn2_1a. \\ & \nearrow & & & \\ & & B_{2u} & & \end{array}$$

This result obviously shows that the formation of dipolar clusters—probably of dynamical character—in RbAS-70 starts below 220 K, i.e. below the PT temperature of pure AS. Thus, short-range ferroelectric order appears in RbAS-70 below 220 K, while the orthorhombic symmetry of the disordered phase is preserved on average, because the low-frequency lattice modes of the SO_4^{2-} ions do not exhibit any changes in long-range order on cooling.

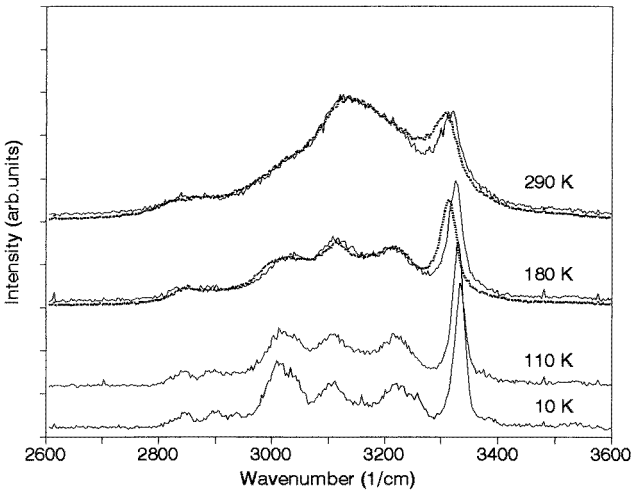

Figure 13. The temperature evolution of the stretching internal modes ν_1^N and ν_3^N in RbAS-10 (dotted line) and RbAS-70 (solid line) observed for the $Y(ZZ)X$ scattering geometry.

4.2.3. Internal modes of NH_4^+. The Raman spectra of the ν_1^N and ν_3^N stretching modes in RbAS-70 versus temperature are shown in figure 13, where broken lines correspond

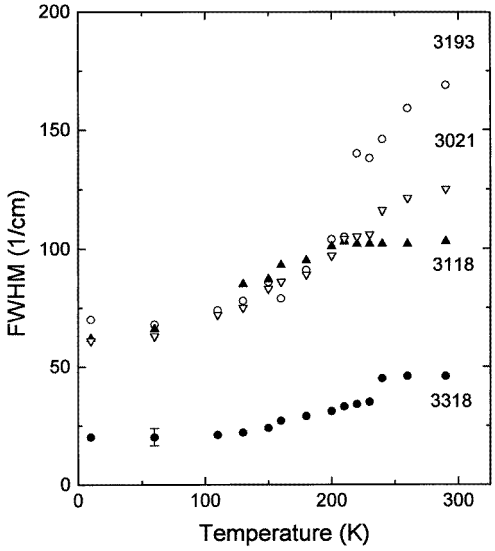

Figure 14. The temperature dependence of the half-widths (FWHM) of the component peaks in the spectra of RbAS-70 of figure 13. The numbers refer to room temperature values of the peak frequencies. The uncertainty in the frequency values is indicated by the error bars.

to the spectra of RbAS-10 (taken under the same experimental conditions and in the same scattering geometry), multiplied by a factor of 0.3 according to the ammonium concentration ratio. Below 3300 cm^{-1} the observed spectra are practically identical for the two samples in the paraelectric phase at 290 K as well as at 180 K, where the ferroelectric state in RbAS-10 occurs. The high-frequency ν_3^N component is centred at 3307 cm^{-1} for RbAS-10 and shifts up to 3318 cm^{-1} for RbAS-70, apparently due to stronger distortion of ammonium ions in RbAS-70. The temperature dependences of the linewidths (FWHM) in the ν_1^N–ν_3^N range ascertained from multi-Lorentzian fits are shown in figure 14. The abrupt narrowing of the ν_3^N component located at 3193 cm^{-1} (the room temperature value) together with a poorly resolved step for the 3318 cm^{-1} component confirm the occurrence of short-range dipolar correlations near 220 K in RbAS-70.

5. Conclusions

To conclude, let us summarize our principal findings.

(i) The Raman spectra of SO_4^{2-} internal modes reveal pseudo-hexagonal crystal structure, known to occur for pure AS, even in mixed crystals.

(ii) The presence of ammonium induces disorder in the sulphate sublattice, which is manifested by the emergence of a strong broad central peak in the room temperature A_g Raman spectra of RbAS-10. This contribution could be well modelled by a Debye relaxator. On cooling, a phase transition with lattice dynamics analogous to that of pure AS is observed in RbAS-10: both the central component (relaxator) and the 44 cm^{-1} mode vanish.

(iii) Comparative analysis of the internal modes of NH_4^+ in the room temperature phase and on lowering the temperature reveals the occurrence of local correlations of ferroelectric type in RbAS-70 just below the phase transition temperature of pure AS. Evidence for this is provided by the observation of changes in the spectra, which are compatible with the

selection rules of the ferroelectric phase.

(iv) Raman spectroscopy allowed us to determine the very beginning of the dipolar cluster formation in RbAS-70 below 220 K. All signs of the short-range ferroelectric order, which appears below 220 K and indicates the onset of a dynamic dipolar glass transition, develop gradually on further cooling and become saturated at about 150 K. Below this temperature, only a dielectric dispersion was observed (De Sousa Meneses *et al* 1996a, b) in the frequency range below 220 MHz; this range evidently appears static from the viewpoint of Raman scattering.

Acknowledgments

The work was partially supported by the Russian Foundation of Basic Research (Projects N96-02-16271 and N97-02-17878) and by the Grant Agency of the Czech Republic (Project No 202/95/1393). Constant stimulating support from A Lebrun (INSSET–Université de Picardie) was much appreciated.

References

Ahmed S, Shaman A M, Kamel R and Badr Y 1987 *Phys. Status Solidi* a **99** 131
Carter R L 1976 *Spectrochim. Acta* A **32** 575
De Sousa Meneses D 1995 *Solid State Commun.* **96** 5
De Sousa Meneses D, Hauret G, Simon P, Brehat F and Wyncke B 1995 *Phys. Rev.* B **51** 2669
De Sousa Meneses D, Simon P, Hauret G and Maglione M 1996a *Europhys. Lett.* **36** 461
De Sousa Meneses D, Simon P and Maglione M 1996b *Ferroelectrics* **176** 61
Hasebe K 1981 *J. Phys. Soc. Japan* **50** 1266
Iqbal Z and Christoe C W 1976 *Solid State Commun.* **18** 269
Kozlov G V, Lebedev S P, Volkov A A, Petzelt J, Wyncke B and Brehat F 1988 *J. Phys. C: Solid State Phys.* **21** 4883
Montero S, Schmolz R and Haussuhl S 1973 *J. Raman Spectrosc.* **2** 101
Nakamoto K 1986 *Infrared and Raman Spectra of Inorganic and Coordination Compounds* (New York: Wiley)
Ohi K, Osaka J and Uno H 1978 *J. Phys. Soc. Japan* **44** 529
Petzelt J, Grigas J and Mayerová I 1973 *Ferroelectrics* **6** 225
Sawada A, Makita Y and Takagi Y 1976 *J. Phys. Soc. Japan* **41** 174
Simon P 1992 *Ferroelectrics* **135** 169
Schlemper E O and Hamilton W C 1966 *J. Chem. Phys.* **44** 4498
Torgashev V I, Latush L T and Yuzyuk Yu I 1992 *Ferroelectrics* **125** 129
Torgashev V I, Yuzyuk Yu I, Burmistrova, Smutný F and Vaněk P 1993 *J. Phys.: Condens. Matter* **5** 5761
Torgashev V I, Yuzyuk Yu I, Rabkin L M, Durnev Yu I and Latush L T 1991 *Phys. Status Solidi* b **165** 305
Torgashev V I, Yuzyuk Yu I, Rabkin L M and Fedosyuk R M 1988 *Kristallografiya* **33** 143
Torrie B H, Lin C C, Binbrek O S and Anderson A 1972 *J. Phys. Chem. Solids* **33** 697
Unruh H-G, Kruger J and Sailer E 1978 *Ferroelectrics* **20** 3
Venkateswarlu P, Bist H D and Jain Y S 1975 *J. Raman Spectrosc.* **3** 143
Yuzyuk Yu I, Gregora I, Vorlíček V and Petzelt J 1996 *J. Phys.: Condens. Matter* **8** 619
Yuzyuk Yu I, Gregora I, Vorlíček V, Pokorný J and Petzelt J 1995 *J. Phys.: Condens. Matter* **7** 683